Specifying PML Conductivities by Considering Numerical Reflection Dependencies

Scott C. Winton and Carey M. Rappaport, *Senior Member, IEEE*

***Abstract*—Berenger's perfectly matched layer (PML) absorbing boundary condition (ABC) has greatly enhanced finite-difference time-domain (FDTD) scattering analysis. In a discretized domain, however, performance is signal-dependent and large-angle performance is poor due to a rapid reduction in layer decay rate. Increasing the conductivity to offset this reduction increases the discretization errors, especially at near-normal incidence angles. However, by carefully specifying the conductivity in each of the PML sublayers, it is possible to balance the small and large angle performance. The signal-dependence of reflections may be described in terms of the number of spatial points per wavelength. This lends itself to an overall strategy for which to search for PML profiles that provide superior performance for waves incident on a PML at angles between 0–75° and signals that have at least 15 spatial points per wavelength sampling. A one-dimensional (1-D) projection method may be employed to allow an exhaustive search to become a viable alternative to optimization. Such a search provides profile parameters that, while not necessarily "optimal," give excellent wide-angle wide-band reflection performance.**

***Index Terms*—Finite-difference time-domain (FDTD) methods, perfectly matched layers (PMLs).**

I. Introduction

THE finite-difference time-domain (FDTD) method for electromagnetic scattering problems is particularly useful because it is wide band, easily implemented, and adaptable to a wide variety of problems. To keep FDTD simulations from becoming computationally expensive, edges of the computational domain must be kept as close to the scatterer as possible. To avoid reflections from the edges of the domain from scattered fields propagating in all directions, an absorbing boundary condition (ABC) must absorb waves incident from all angles. Historically, ABCs have had only limited success in absorbing waves incident at all angles [2]–[5], but this recently changed with the introduction of the Berenger perfectly matched layer (PML) [6].

The PML works perfectly in continuous analysis, absorbing waves incident at arbitrary angles with arbitrary attenuation. Unfortunately, in order to be used in computer simulations, the PML must be discretized. This discretization limits the conductivity increase for offsetting the reduction in decay rate as the angle of incidence increases and thus limits the overall performance of the PML. Although many efforts improve the PML [7]–[15], few of these deal with performance as a function of angle, choosing instead to concentrate on improving performance at normal incidence. Although large angle effects may be minor if waves incident on a PML at grazing angles reflect nearly normally incident on an adjacent PML, it has been shown [7] that there are several applications where this is not the case and that the performance at large incidence angles is important to the overall performance of the ABC. Consequently, the improvement of large angle performance of the PML is an important problem.

Discretization also prevents the PML from being signal-independent, as it is in the continuous case. Most investigators choose to describe this signal-dependence as a function of frequency. Because FDTD involves spatial and temporal sampling, we suggest that it may be simpler to describe the signal-dependence in terms of spatial points per wavelength.

There has also been much effort to analyze numerical reflecticans in the PML in order to optimize [16]–[20] wave absorption. Obtaining a closed-form expression for the reflection from a PML as a function of the PML parameters, however, is a difficult problem. This difficulty lies in the fact that numerical reflections are created each time a wave passes from one layer to another. These reflections, in turn, create more reflections as they encounter different layers. Keeping track of all reflections becomes increasingly difficult as the number of layers is increased. Furthermore, this type of analysis can only be performed for one frequency at a time, complicating any effort for optimization.

The approach being used for this current work is largely heuristic. We wish to understand the mechanisms that affect reflections from a PML in order to develop a strategy that will allow us to identify PML parameters that will provide enhanced performance over the widest range of angles and signals. With the aid of computational analysis tools, an automated search has been developed for PML parameters . Although the "optimal" piofile may depend on the specific application, the parameters determined in this analysis provide the best wide-band wide-angle performance reported in the standard literature.

II. Reflection Dependencies

The decay rate of the PML in continuous time and space is given as $\alpha = \sigma\eta_0 \cos\theta$ [9], where θ is the incidence angle, σ is the conductivity of the PML , and η_0 is the impedance of free-space. Note that the decay rate is proportional to $\cos\theta$. Since there is no reflection at the PML interface, σ may be chosen arbitrarily large in order to offset the loss of decay rate due to the $\cos\theta$ factor.

The geometry for the discrete PML is shown in Fig. 1 The decay rate in the discretized PML also decreases with increasing

Manuscript received December 10, 1997; revised May 4, 2000.

S. C. Winton is with the Mitre Corporation, Bedford, MA 01730-1420 USA.

C. M. Rappaport is with the Center for Electromagnetics Research, Northeastern University, Boston, MA 02115 USA.

Publisher Item Identifier S 0018-926X(00)06943-X.

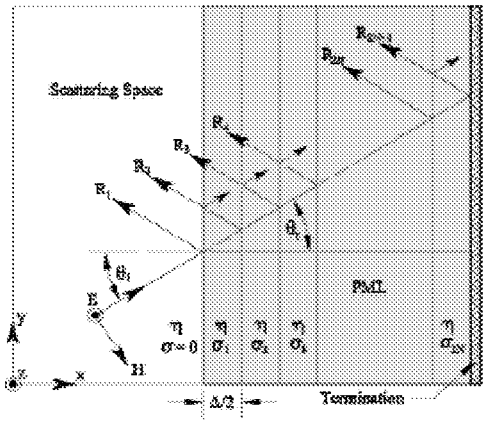

Fig. 1. Lattice geometry and typical plane wave incident on N-layer conductivity profiled PML ABC.

angle. Unlike with the continuous case, the discretized σ_i in the ith PML sublayer may not be chosen arbitrarily large. In general, since FDTD simulations calculate electric and magnetic fields on complementary overlapping lattices, they are sensitive to changes in the parameters of adjacent layers. Stated another way, at any air-PML or PML–PML interface, the discreta equations for the fields at the interface are dependent on unmatched conductivities.

As an example, assume that σ_i are constant over a PML half-space. An incident wave encounters only one interface: that between free-space and the PML. The difference equation for the field at the interface will be dependent on the conductivity of the free-space ($\sigma = 0.0$) and the conductivity of the PML ($\sigma =$ constant). If σ is very small, the resulting reflection will also be very small. If σ is increased, the decay rate increases, but there will also be a larger reflection from the interface. If a Gaussian pulse Exp$[-c^2(t-t_0)^2/W^2]$, where t_0 is the time at which the pulse is at its maximum, excites the first row of an FDTD grid, Fig. 2 shows the total reflection from a constant conductivity PML half-space versus angle for values of σ equal 0.15, 0.3, and 0.45 S/m. For these simulations, the temporal increment $\Delta t = 10$ pS, spatial increment $\Delta = 0.012$ m and $W = (50/3)\Delta = 0.2$ m. It is apparent that the reflection increases with an increase in σ and that as θ increases the discrete change in conductivity at the interface is moderated and the reflection decreases.

It should be noted that the time and space steps need not have physical units. Instead, the entire FDTD simulation including the PML may be entirely specified by the Courant number $R = c\Delta t/\Delta$ and the ith layer decay rate $S_i = \sigma_i \Delta \eta_0$ and the performance of the PML may be parameterized in terms of two unitless parameters: $S = (S_1, S_2, \ldots, S-N)$, λ/Δ and the angle of incidence, θ. Given these, Δ and the wave phase velocity all other physical quantities can be determined.

One way reflection from the PML is reduced is to vary the sublayer conductivities from small values near the free space interface to larger values toward the final sublayer. This profiling of PML conductivity improves absorption, providing an alternative to increasing the number of sublayers, which is computationally expensive. Since incoming waves do not encounter larger values of σ until well within the layer, the reflections caused by these larger jumps in conductivity are attenuated by the initial lossy layers both for forward and backward propagation. Yet even with the parabolic conductivity profile $\sigma_i = \sigma_f(i/N)^2$ [6], the total reflection from an eight PML at 75° incidence is shown to be about -33 dB, compared to the -100 dB achieved at normal incidence. It is noted that as the angle of incidence is increased, the numerical experimental results more closely match the theoretical loss, which, for the case of [6] at 75°, was -31 dB. This can be explained by the fact that as the angle of incidence is increased, the projected spatial increment $\Delta \cos\theta$ decreases, which has the effect of decreasing the discretization error; the jumps in conductivity variations at every layer interface are smaller, giving lower sublayer reflections.

Since $\sigma^*/\mu_0 = \sigma/\epsilon$, where σ^* is the magnetic conductivity, σ/ϵ may be used in both Ampere's and Faraday's laws [13]. Discrete conductivity values σ_n can be assigned to every half sublayer. Using the half-layer profile specification and assuming no discretization error, the two-way loss equation is

$$L = e^{-2\sum_{n=1}^{2N} \sigma_n \eta_0 \cos\theta \frac{\Delta}{2}} \tag{1}$$

with conductivity profile taking the form $\sigma_n = \sigma_f(n/2N)^p$, $n = 1, 2, \ldots 2N$. For this profile form, the decay rate S may be described by $S_f = \sigma_f \Delta$ and p. A conductivity profile with a power dependence is simple to implement and does not change as rapidly as a profile with an exponential dependence, which was found to not perform as well.

The three different time-domain signals shown in Fig. 3 have different temporal increments (Sig.1 $\Delta t = 2$ ps, Sig.2 $\Delta t = 1.8$ ps, Sig.3 $\Delta t = 1.7$ ps), as well as the different waveforms, which account for the different frequency contents. These signals have been used as the excitation for a one-dimensional (1-D) FDTD simulation to test various PML's with perfectly conducting terminations. In each case, the Fourier transform of the reflected field divided by the Fourier transform of the incident field has been plotted versus the inverse of the discrete frequency $2\pi/\omega\Delta t$ times the Courant number R, which is also the number of spatial points per wavelength λ/Δ. The use of nonphysical units to describe PML reflection has also been used in [22]. The incident waveform was obtained by using a much larger FDTD simulation, where the wave passes over the receiver location just outside the PML and the simulations is stopped before reflection can occur. Results for the 1-D FDTD simulations at normal incidence in Fig. 4 show all three signals practically overlapping for all three PML layer configurations of $N = 8, 10, 12$. The layer size and normalized conductivity profile is indicated for each set of graphs. Note that since the curves coincide for each PML configuration, PML reflections are independent of R and of the waveform, but dependent primarily on the relationship between the two (i.e., λ/Δ).

To further investigate the PML reflection dependencies, we consider the same three signals, but in this case maintain the temporal increment and conductivity profile, but use three different spatial increments and, hence, different Courant numbers and different values of the decay rate S. Here we test the

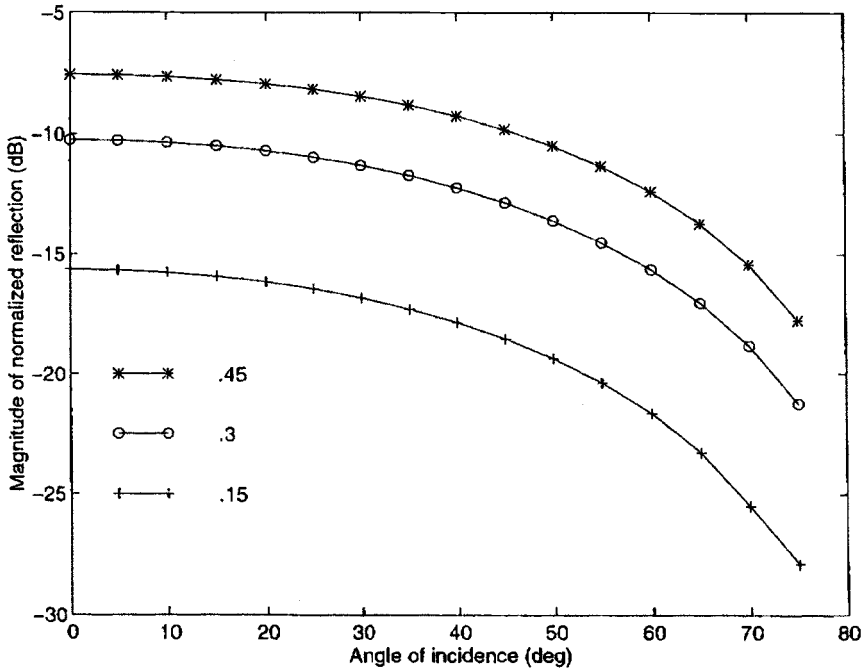

Fig. 2. Reflection as a function of angle for PML half-spaces with constant conductivity profile $\sigma_c = 0.45\ (*)$, 0.30 $(\circ)$, and 0.15 $(+)$.

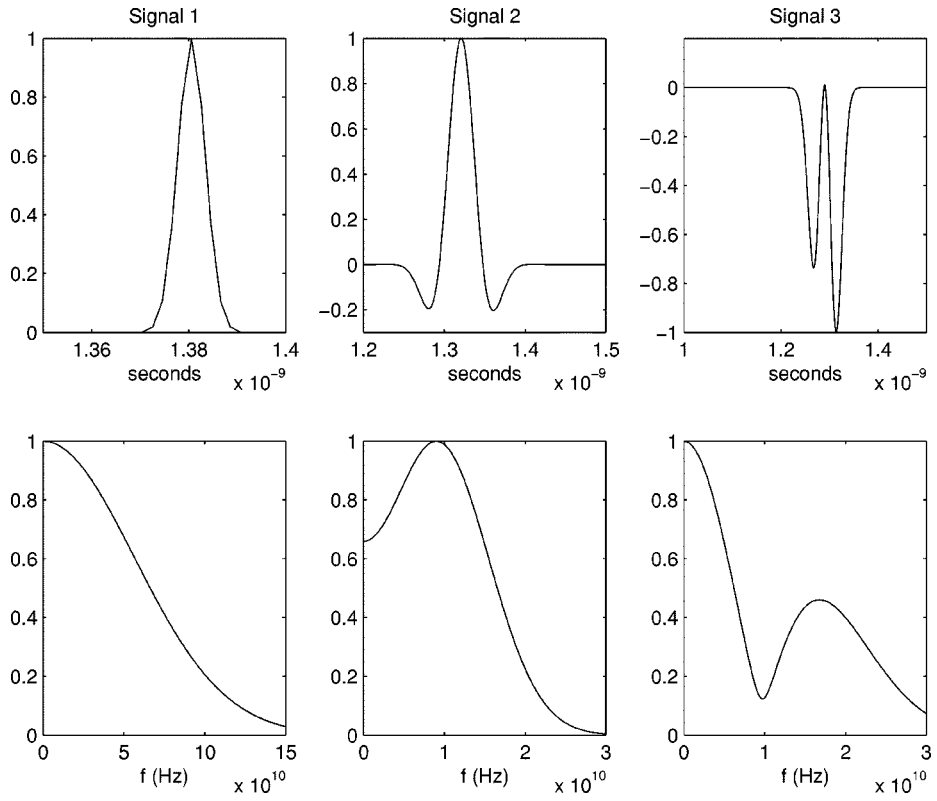

Fig. 3. Three time-domain signals and their associated power spectral densities. For Signal 1 $\Delta t = 2$ ps; Signal 2 $\Delta t = 1.8$ ps; Signal 3 $\Delta t = 1.7$ ps.

eight-layer PML only; the results are in Fig. 5. Note that the magnitudes of the reflection coefficients for the different signals are very different.

These figures clearly indicate that it is not the physical quantities ω and σ that determine the reflection from the PML, but rather the nonphysical quantities S and λ/Δ. This intuitive result follows since the PML works "perfectly" in the continuous domain specified by physical parameters, while reflections that arise from the discretized PML depends on discretization parameters.

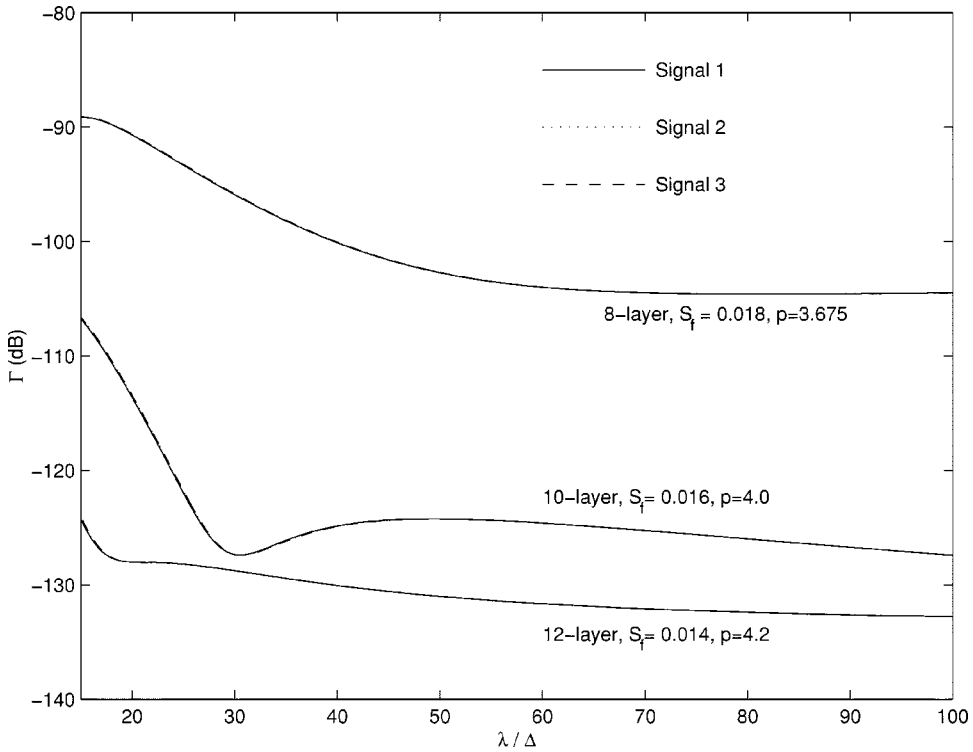

Fig. 4. Reflection coefficient as a function of λ/Δ for various PMLs as determined using three different signals. $\Delta = 0.6$ mm. Signal 1 (-) ($\Delta t = 2$ ps); Signal 2 (..) ($\Delta t = 1.8$ ps); Signal 3 (–) ($\Delta t = 1.7$ ps).

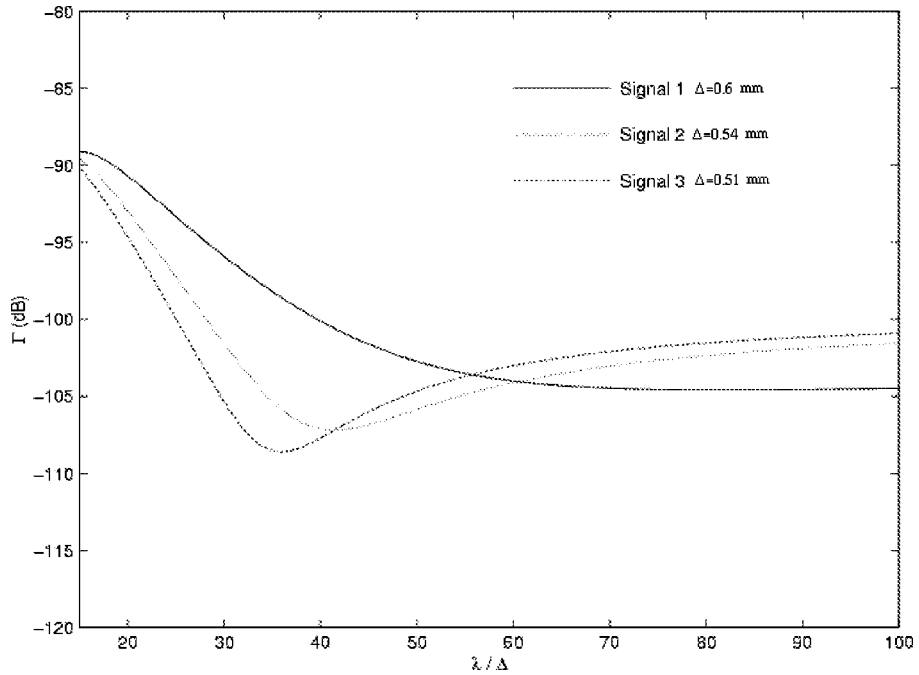

Fig. 5. Reflection coefficient as a function of λ/Δ for various PMLs as determined using three different signals. Signal 1 (-) ($\Delta t = 2$ ps, $\Delta = 0.6$ mm, $S_f\Delta = 0.018$, $p = 3.675$); Signal 2 (..) ($\Delta t = 1.8$ ps, $\Delta = 0.54$ mm, $S_f\Delta = 0.0162$, $p = 3.675$); Signal 3 (–) ($\Delta t = 1.7$ ps, $\Delta = 0.51$ mm, $\sigma_f\Delta = 0.0153$, $p = 3.675$).

III. Exhaustive Search versus Optimization

One obvious method for improving PML performance is to optimize the PML parameters S_f and p over all angles and signals. To do this would require an analytic expression for reflections from the PML as a function of the size of the PML, incident angle, incident signal, S_f, and p. Such analytic expressions which have been numerically verified for small N PMLs appear in the literature [18], [22]. For an eight-layer PML, analytic expressions in the literature have not been found to accurately predict numerical reflections for all angles and incident waveforms.

Even assuming confidence with an analytic expression of the reflection coefficient, optimization of the PML over all profiles, signals, and angles is a nontrivial problem. By relaxing the "optimality" requirement, we may utilize an exhaustive search to identify profiles that will provide superior performance over a wide range of signals and angles.

IV. Exhaustive Search

The basic idea behind the exhaustive search is simple: FDTD simulations are run for each PML profile under consideration. The search continues until suitable profile parameters have been identified. Because we must account for both the angle dependence and signal dependence, however, steps must be taken to make the search viable and manageable.

Having described the PML signal dependence, we now consider angle dependence. Similar to an optimization problem, we must create a criterion on which to judge the results. Furthermore, recall that the decay rate α in the PML is given as $\alpha = \sigma\eta_0 \cos\theta$. Therefore, regardless of the profile, we can expect significant reflection from a PML with a perfectly conducting termination at very large angles. It is therefore appropriate to introduce a weighting function. To improve large angle performance without sacrificing near-normal performance, we have chosen the simple "minimax" criteria with a weighting function

$$C(S_f, p, \lambda/\Delta) = \max_{\theta} \{|\Gamma(\theta, \sigma_f, p, \lambda/\Delta)W(\theta)|\} \tag{2}$$

where $W(\theta)$ is a weighting function and $\Gamma(\theta, \sigma_f, p, \lambda/\Delta)$ is the reflection from the PML. Note that C is not a function of θ. We seek the values of S_f and p that minimize C. This function is well suited to the wide-angle minimum reflection because it does not penalize for a realization of $\Gamma(\theta)$ that has a large variation. The weighting function $W(\theta)$ is equal to unity (0 dB) up to and including 60°, at which point it drops off at -12 dB/5° to a minimum of -36 dB at 75°. This dropoff from 60° to 75° accounts for the reduction in performance predicted by (1). Incident angles larger than 75° are not considered.

To deal with the signal dependence, we describe reflection as a function of spatial points per wavelength and break incident signals into three groups. These groups have, respectively, a minimum of 15, 20, and 30 spatial point per wavelength sampling for frequencies that have power densities within -6 dB of the maximum power density. The results reported in this work are, therefore, worst-case reflections for signals adhering to these groups.

V. One-Dimensional Projection Method

Running a two-dimensional (2-D) FDTD simulation for every S_f and p is time prohibitive. Furthermore, depending on the type of excitation used, analysis of the reflection at a single angle is quite complicated. Fortunately, it has been shown that 2-D uniform plane waves may be represented using 1-D FDTD simulations [21]. Reflections from a PML may also be analyzed using 1-D FDTD simulations. Basically, a 1-D "slice" of a 2-D wave is taken in the direction normal to the PML under test. This 1-D wave moves with a velocity $c/\cos\theta$, where c is the velocity of the 2-D wave in the propagation direction perpendicular to the planar wavefront. The PML only attenuates in the direction normal to its interface, so there are no transverse variations in the PML, but since the normal variations are specified by the same FDTD formalism as the 2-D, the 1-D FDTD simulation efficiently demonstrates the complete reflection and transmission characteristics of the PML.

This can be shown analytically. It has been shown [13] that the time harmonic curl equations for TM waves inside a continuous PML may be written as

$$-\frac{\partial E_z}{\partial y} = j\omega\mu_0 H_x \tag{3a}$$

$$\frac{\partial E_z}{\partial x}\left(\frac{1}{1 - j\sigma/\omega\epsilon_0}\right) = j\omega\mu_0 H_y \tag{3b}$$

$$\frac{\partial H_y}{\partial x}\left(\frac{1}{1 - j\sigma/\omega\epsilon_0}\right) - \frac{\partial H_x}{\partial y} = j\omega\mu_0 E_z. \tag{3c}$$

The time-harmonic plane wave solution for (3) is of the form

$$E_z = E_0 e^{-jk_x^{pml}x - jk_y y + j\omega t} \tag{4a}$$

where the time dependence $e^{j\omega t}$ will be suppressed in the following:

$$\mathbf{H} = \frac{E_z}{\eta_0}(\hat{x}\sin\theta - \hat{y}\cos\theta) \tag{4b}$$

with

$$\begin{aligned} k_x^{pml} &= k_x\left(1 - j\frac{\sigma}{\omega\epsilon_0}\right) \\ &= \left(\frac{\omega}{c} - j\sigma\eta_0\right)\cos\theta. \end{aligned} \tag{5}$$

Note that the velocity of the 1-D slice inside the PML is $c/\cos\theta$. So the 1-D solution should take the form

$$E_{1D_{pml}} = \hat{z}E_z \tag{6a}$$

$$H_{1D_{pml}} = \hat{y}H_y \tag{6b}$$

at $y = \theta$.

Because the solution in (6) does not satisfy Maxwell's curl equations, Ampere's Law must be modified. Taking the partial derivative of H_x and H_y from (4b) with respect to y and x, respectively, at $y = 0$, with $k_y = (\omega/c)\sin\theta$ gives

$$\frac{\partial H_x}{\partial y} = -jk_0(\sin^2\theta)\frac{E_o}{\eta_0}e^{-jk_x^{pml}x} \tag{7a}$$

$$\frac{\partial H_y}{\partial x} = jk_0(\cos^2\theta)(1 - j\sigma/\omega\epsilon_0)\frac{E_o}{\eta_0}e^{-jk_x^{pml}x}. \tag{7b}$$

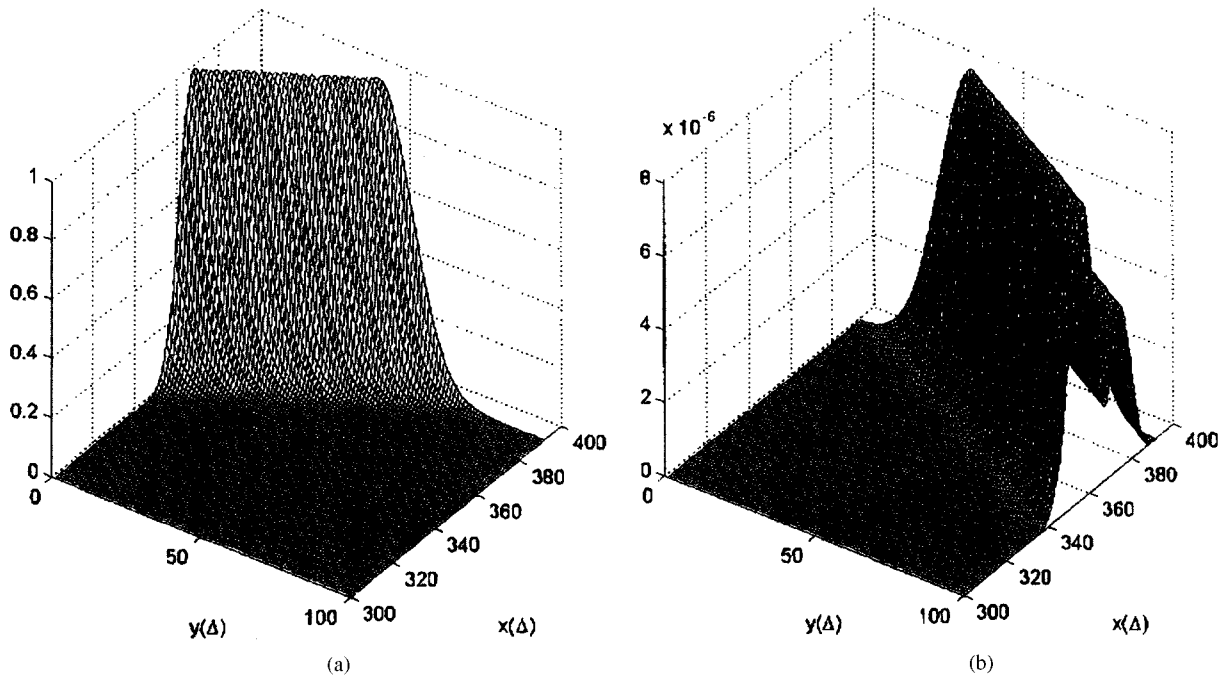

(a) (b)

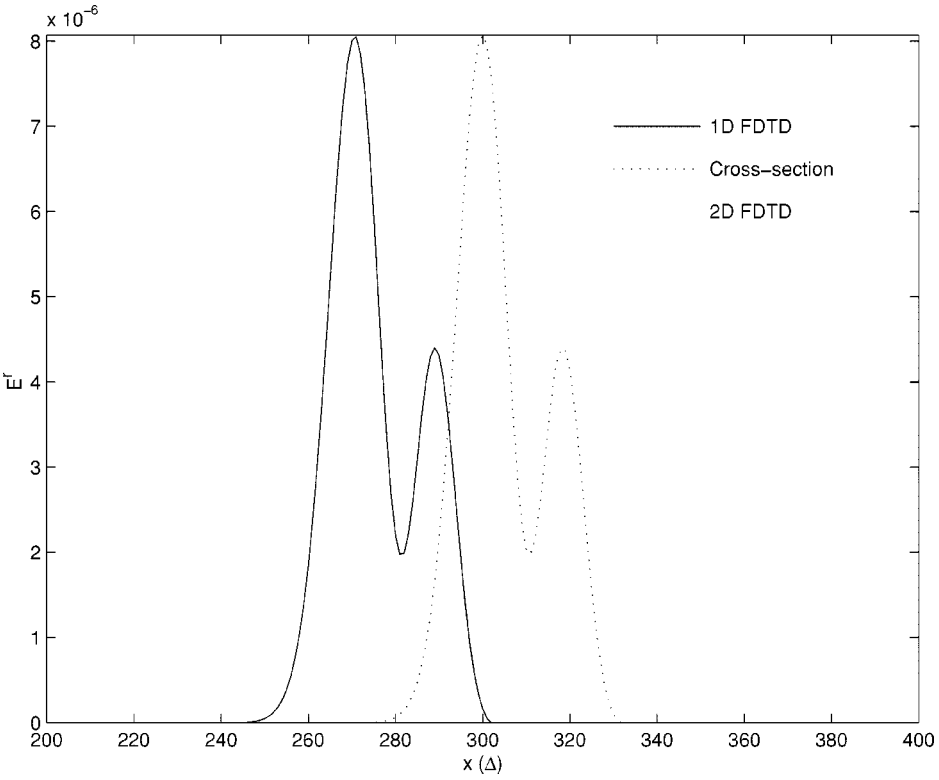

(c)

Fig. 6. Gaussian plane wave incident on an eight-layer PML located at $x = 392\Delta$ at 30° (from lower right to left). These are views of a portion of a 400 × 100 grid. (a) Incident field. (b) Scattered field showing specular reflection from PML five orders of magnitude lower than the incident field. Time slice of graphs in (c) +150 time steps of those in (a) and (b). (c) Cross-section of reflected field from 2-D simulation and reflected field from 1-D simulation. Time slice of graphs in (c) +150 time steps of those in (a) and (b).

These are equated as

$$\frac{\partial H_x}{\partial y} = \frac{-(1-\cos^2\theta)}{\cos^2\theta(1-j\sigma/\omega\epsilon_0)}\frac{\partial H_y}{\partial x}.$$

Thus, the left-hand side of (3c) becomes

$$\frac{1}{\cos^2\theta(1-j\sigma/\omega\epsilon_0)}\frac{\partial H_y}{\partial x}.$$

Now (3) for the 1-D curl equations in the time domain becomes

$$\frac{\partial E_{z1Dpml}}{\partial x} = \mu_0 \frac{\partial H_{y1Dpml}}{\partial t} + \frac{\sigma \mu_0}{\epsilon_0} H_{y1Dpml} \quad (8a)$$

$$\frac{1}{\cos^2 \theta} \frac{\partial H_{y1Dpml}}{\partial x} = \epsilon_0 \frac{\partial E_{z1Dpml}}{\partial t} + \sigma E_{z1Dpml}. \quad (8b)$$

Equation (8) should be recognized as the lossy Faraday and Ampere laws with an impedance η^{pml} matched to that of free-space $\sqrt{\mu_0/\epsilon_0} = E_z/H_y$.

It can be shown that there are 1-D equivalents for TE waves inside the PML as well. The derivation proceeds along similar lines.

To verify the proceeding derivation, we have run 2-D FDTD simulations and compared them with the 1-D equivalents. The results are found in Fig. 6. In Fig. 6, a TM plane wave incident at 30° is partially absorbed by an eight-layer PML at the back wall. The incident wave is propagating toward the left rear corner. Fig. 6(b) shows the reflected field. Note that the incident and reflected fields obeys Snells's law and that the reflected field is several orders of magnitude smaller than the incident field. Fig. 6(c) shows a cross section of the reflected field from the 2-D grid taken at 50Δ from the right-hand side as well as the reflected field from 1-D simulation. The time stamp of the plots of Fig. 6(c) are 150 timesteps from those of Fig. 6(b). Note the similarities in the pulse shape and amplitude. The 2-D plane wave was created by using 1-D FDTD simulations on the left- and right-hand sides of the grid as described in [21]. The absence of additional reflection artifacts along the left and right sides indicate that the existing reflected field is generated from the PML only.

The 1-D method comprises a simple and efficient means to test PML reflections. The attenuation is in one direction, the direction normal to the boundary. A careful dispersion analysis shows that the error from representing a 2-D wave with a 1-D slice is comparable to the error involved in numerical dispersion which is inherent to 2-D FDTD simulations. In two dimensions, Maxwell's curl equations for the PML require either a supplemental equation, as used in [13] or split-field equations as used by [6].

Armed with this powerful tool, the search for S_f and p is greatly simplified and, hence, can be automated. A search program may iterate through different values of θ, S_f and p. Furthermore, since reflections can be described in terms of spatial points per wavelength, we may use a single wide-band incident wave as a test signal and be able to account for the signal dependence of the PML as described in the previous sections.

VI. Results

Using the techniques described in the previous sections, several automated searches were performed to identify the PML profile parameters S_f and p that will yield superior performance.

For each profile tested, a 1-D FDTD simulation was run for every angle between and including 0° and 75° at 5° increments.

TABLE I
EIGHT-LAYER PML

λ/Δ	S_f	p	Γ (dB)
15	0.0152	3.77	-90.27
20	0.0160	3.74	-93.71
30	0.0177	3.78	-98.83

TABLE II
TEN-LAYER PML

λ/Δ	S_f	p	Γ (dB)
15	0.0215	3.93	-106.17
20	0.0179	3.99	-108.95
30	0.0193	6.98	-114.17

TABLE III
TWELVE-LAYER PML

λ/Δ	S_f	p	Γ (dB)
15	0.026	4.20	-119.69
20	0.020	4.50	-122.37
30	0.021	4.40	-127.29

TABLE IV
FOURTEEN-LAYER PML

λ/Δ	S_f	p	Γ (dB)
15	0.020	4.70	-130.73
20	0.023	5.00	-138.12
30	0.023	5.00	-138.12

In each case, a wide-band test signal was the incident wave. The reflection coefficient is calculated by

$$|\Gamma(\lambda/\Delta)| = 20 \log \max \left\{ \left| \frac{fft(E^s)}{fft(E^i)} \right| W(\theta) \right\}$$

where

$\Gamma(\lambda/\Delta)$ reflection;
E^s scattered field;
E^i incident field.

Our experiments indicate that $\Gamma(\lambda/\Delta)$ becomes nonincreasing after a certain value of points per wavelength, usual

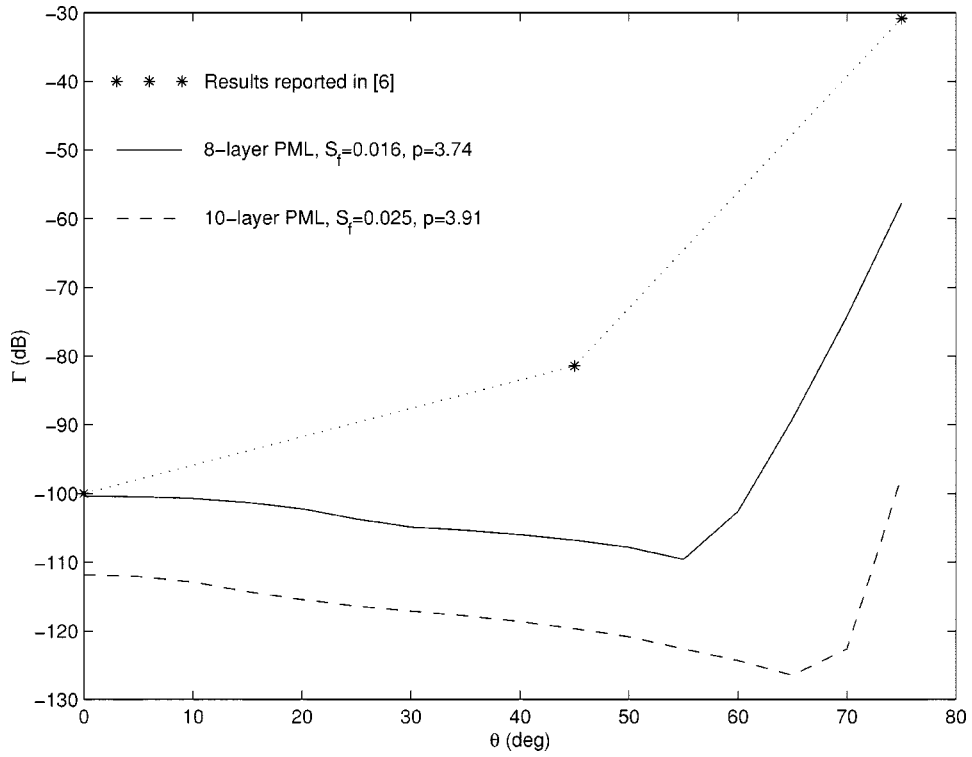

Fig. 7. Reflection coefficients of N-layer PMLs as a function of θ. $(N,\ p,\ \sigma_f\Delta) = (8,\ 3.74,\ 0.016)$ (–), $(10,\ 3.91,\ 0.025)$ (- -) and the results reported in [6] $(*)$. The values of W and Δ used in the simulations were chosen to match those used in [6].

between 100 and 150. Therefore, once $\Gamma(\lambda/\Delta)$ has been calculated for a given profile and angle, the maximum between 15, 20, 30, and 200 points per wavelength, respectively, are recorded. Then these maxima are multiplied by the weighting function as necessary to yield the overall maximum for a given profile. The parameters that yield the smallest overall maximums are found in Tables I–IV.

As the results reported in the tables are "worst case" for the discrete frequency with the greatest reflection, depending on the incident time-domain signal, results may be significantly better than those reported in the tables. For example, a Gaussian pulse with a $10\Delta t$ time constant has been used as the incident signal to test plane waves incident on the PML at various angles for some of the profiles found in Tables I and II. This is the same test signal used in [6]. The reflections coefficient as calculated by

$$|\Gamma| = 20 \log \max_{\theta} \left| \frac{E^s}{\max_t E^i} \right|$$

have been plotted versus angle in Fig. 7 for the eight-layer PML with conductivity profile parameters $S_f = 0.016$ and $p = 3.74$. The results reported by Berenger [6] have also been plotted. Note that there is more than an order of magnitude improvement at both 45° and 75°. Using the same test signal, the reflection coefficient for a ten-layer PML with conductivity profile parameters $S_f = 0.025$ and $p = 3.91$ has also been plotted on Fig. 7. Using an additional two layers, we may further decrease $\Gamma(\theta)$ by 2 orders of magnitude at 75°.

The improved performance shown by the ten-layer PML at large angles suggests that the weighting function may not be needed for larger PMLs. To explore this idea, several additional searches were performed without including the weighting function, the results for these searches are found in Tables V–VII. Although the results for searches that do not employ the weighting function are not quite as good overall, these profiles provide excellent performance across the entire range of 0°–75°.

TABLE V
TEN-LAYER PML NO WEIGHTING

λ/Δ	S_f	p	Γ (dB)
15	0.0260	3.90	-102.30
20	0.0295	3.90	-106.42
30	0.0345	3.90	-107.43

TABLE VI
TWELVE-LAYER PML NO WEIGHTING

λ/Δ	S_f	p	Γ (dB)
15	0.0270	4.2	-116.64
20	0.0305	4.1	-120.83
30	0.0365	4.1	-122.49

TABLE VII
FOURTEEN-LAYER PML NO WEIGHTING

λ/Δ	S_f	p	Γ (dB)
15	0.028	4.5	-129.13
20	0.028	4.5	-129.13
30	0.031	4.9	-132.66

VII. CONCLUSION

We have explored the mechanisms that govern reflection form PML absorbing boundaries. In so doing, we have presented a simple means of accounting for the signal dependence of PML reflections. Furthermore, we have shown that it is the "discrete" parameters points per wavelength λ/Δ and loss per PML sublayer S, which govern this signal dependence and not the "physical" parameters ω and σ.

We have presented a fast and simple method to determine the reflection from a PML due to uniform plane wave at arbitrary angle. This method does not require the use of an anisotropic media or a split-field formulation. Plane wave decomposition may be used to gain insight into the overall reflection from arbitrary waves.

Employing these methods, we have conducted searches for conductivity profiles that provide improved performance. Assuming adequate sampling, profile parameters have been provided that will insure exceptional performance over a wide variety of scattering problems. This approach removes the burden of seeking adequate ABC absorption from the FDTD user.

Despite the obvious utility of the method, caution must be exercised to ensure that extreme angles ($>75°$) are minimized. The method developed here also does not account for evanescent waves.

ACKNOWLEDGMENT

The authors would like to thank A. W. Morgenthaler and E. L. Miller for many helpful discussions.

REFERENCES

[1] K. S. Yee, "Numerical solution of initial boundary-value problems involving Maxwell's equations in isotropic media," *IEEE Trans. Antennas Propagat.*, vol. AP-14, pp. 302–307, May 1966.
[2] B. Engquist and A. Majda, "Absorbing boundary conditions for the numerical simulation of waves," *Mathematical Computat.*, vol. 31, pp. 629–651, 1977.
[3] G. Mur, "Absorbing boundary conditions for the finite-difference approximation of the time-domain electromagnetic-field equations," *IEEE Trans. Electromagn. Compat.*, vol. EMC-23, pp. 377–382, Nov. 1981.
[4] K. Mei and J. Fang, "Superabsorption—A method to improve absorbing boundary conditions," *IEEE Trans. Antennas Propagat.*, vol. 40, pp. 1001–1010, Sept. 1992.
[5] C. Rappaport and L. Bahrmasel, "An absorbing boundary condition based on anechoic absorber for EM scattering computation," *J. Electromagn. Waves Applicat.*, vol. 6, no. 12, pp. 1621–1634, Dec. 1992.
[6] J. Berenger, "A perfectly matched layer for the absorption of electromagnetic waves," *J. Computat. Phys.*, vol. 114, pp. 185–200, Oct. 1994.
[7] S. Gedney, "An anisotropic perfectly matched layer-absorbing medium for the truncation of FDTD lattices," *IEEE Trans. Antennas Propagat.*, vol. 44, pp. 1630–1639, Dec. 1996.
[8] W. Chew and W. Weedon, "A 3-D perfectly matched medium of modified Maxwell's equations with stretched coordinates," *Microwave Opt. Technol. Lett.*, vol. 7, no. 13, pp. 559–604, Sept. 1994.
[9] C. Rappaport, "Perfectly matched absorbing boundary conditions based on anisotropic lossy mapping of space," *IEEE Microwave Guided Wave Lett.*, vol. 5, pp. 90–92, Mar. 1995.
[10] D. Katz, E. Thiele, and A. Taflove, "Validation and extension to three dimensions of the Berenger PML absorbing boundary," *IEEE Microwave Guided Wave Lett.*, vol. 4, pp. 268–270, Aug. 1994.
[11] M. Gribbon, S. Lee, and A. Cangellaris, "Modification of Berenger's perfectly matched layer for the absorption of electromagnetic waves in layered media," in *Proc. 11th Annu. Rev. Progress Appl. Computat. Electromagn. Symp. Dig.*, Monterey, CA, Mar. 1995, pp. 498–503.
[12] S. Gedney and A. Roden, "The uniaxial perfectly matched layer (UPML) truncations of FDTD lattices for generalized media," in *URSI Symp. Dig.*, Baltimore, MD, July 1996, p. 366.
[13] C. Rappaport, "Interpreting and improving the PML absorbing boundary condition using anisotropic lossy mapping of space," *IEEE Trans. Magn.*, pp. 968–974, May 1996.
[14] Z. Wu and J. Fang, "High-performance PML algorithms," *IEEE Microwave Guided Wave Lett.*, vol. 6, pp. 335–337, Sept. 1996.
[15] L. Gianluca and O. Gandhi, "On the optimal design of the PML absorbing boundary condition for the FDTD code," *IEEE Trans. Antennas Propagat.*, vol. 45, pp. 914–916, May 1997.
[16] Z. Wu and J. Fang, "Numerical implementation and performance of perfectly matched layer boundary condition for waveguide structures," *IEEE Trans. Microwave Theory Tech.*, vol. 43, pp. 2676–2683, Dec. 1995.
[17] J. Wu, R. Lee, and J. Lee, "The use of higher order edge-based finite elements to improve the accuracy of the anisotropic perfectly matched layer," in *URSI Symp. Dig.*, Baltimore, MD, July 1996, p. 361.
[18] J. Fang and Z. Wu, "Closed-form expression of numerical reflection coefficient of perfectly matched layers," in *Proc. URSI Symp. Dig.*, Baltimore, MD, July 1996, p. 364.
[19] "private communication," unpublished, 1996.
[20] Z. Wu and J. Fang, "Closed-form expression of numerical reflection coefficient at PML interfaces and optimization of PML performance," *IEEE Microwave Guided Wave Lett.*, vol. 6, pp. 332–334, Sept. 1996.
[21] S. Winton and C. Rappaport, "Implementation of a two dimensional plane wave FDTD using one dimensional FDTD on the lattice edges," in *Proc.'97 ACES Symp. Dig.*, Monterey, CA, Mar. 1997, pp. 1156–1162.
[22] J. De Moerloose and M. Stuchly, "An efficient way to compare ABC's," *Antennas Propagat. Mag.*, vol. 38, no. 1, pp. 71–75, Feb. 1996.

Scott C. Winton received the B.S. and M.S. degrees in electrical engineering from Northeastern University, Boston, MA, in 1995 and 1999, respectively. He is currently working toward the Ph.D. degree at the same university.

From 1995 to 1999, he was a Research Assistant with Northeastern University and has participated in research involving wave propagation and modeling, scattering, and ground-penetrating radar. In 1999, he joined the Mitre Corporation, Bedford, MA, as an Electromagnetic Compatibility (EMC) Engineer for the Air Force Center.

Mr. Winton is a member of Eta Kappa Nu, Tau Beta Pi, and Phi Kappa Phi honorary societies.

Carey M. Rappaport (S'80–M'87–SM'96) received the S.B. degree in mathematics , in 1982, the S.B., S.M., and E.E. degrees, all in electrical engineering, all in 1982, and the Ph.D. degree in electrical engineering, in June 1987, all from the Massachusetts Institute of Technology (MIT), Cambridge, MA.

From 1981 to 1987, he worked as a Teaching and Research Assistant at MIT and worked during the summers at COMSAT Labs, Clarksburg, MD, and The Aerospace Corporation, El Segundo, CA. He joined the faculty at Northeastern University, Boston, MA, in 1987. He has been Associate Professor of electrical and computer engineering since 1993. During the fall of 1995, he was Visiting Professor of electrical engineering at the Electromagnetics Institute, Technical University of Denmark, Lyngby, as part of the W. Fulbright International Scholar Program. He has consulted for Geo-Centers, Inc., PPG, Inc., and several municipalities on wave propagation and modeling and microwave heating and safety. He has authored over 150 technical journal and conference papers in the areas of microwave antenna design, electromagnetic scattering computation, and bioelectromagnetics and has received two reflector antenna patents and one biomedical device patent.

Dr. Rappaport was awarded the IEEE Antenna and Propagation Society's H. A. Wheeler Award for Best Applications paper of 1985. He is a member of Sigma Xi and Eta Kappa Nu professional honorary societies.